International Journal of GEOMATE, Aug., 2021, Vol.21, Issue 84, pp.112-120
ISSN: 2186-2982 (P), 2186-2990 (O), Japan, DOI: https://doi.org/10.21660/2021.84.j2162
Geotechnique, Construction Materials and Environment

DEVELOPMENT OF A TECHNIQUE FOR OBSERVING THE FROST HEAVING PROCESS IN SOIL USING AN INDUSTRIAL MICRO-FOCUS X-RAY CT SCANNER

Baiyang Song[1], *Dai Nakamura[2], Takayuki Kawaguchi[3]and Shunzo Kawajiri[4]

[1]School of Civil Engineering, Luoyang Institute of Science and Technology, China;
[2,3,4] Faculty of Engineering, Kitami Institute of Technology, Japan

*Corresponding Author, Received: 08 April 2021, Revised: 01 May 2021, Accepted: 12 June 2021

ABSTRACT: This paper aims at developing a technique for observing the frost heaving process in soil nondestructively and microscopically using an industrial micro-focus X-ray CT scanner. For this purpose, a compact frost heaving apparatus that could freeze the soil in one dimension inside the X-ray CT scanner was developed. This experimental method made it possible to observe the process of ice lens formation in the soil and the shape of the ice lens in detail. In highly frost susceptible weathered volcanic ash, ice lenses like multiple cracks were observed to develop in the early stages of the experiment. When the freezing front was stagnant and the heat was balanced, thick and well-developed ice lenses could be observed. The shape of the ice lens observed in the weathered volcanic ash without gravel was relatively flat. In the terrace deposits containing gravel, ice lenses were observed to be formed from around the larger particles. Furthermore, the formed ice lenses were more uneven in shape than weathered volcanic ash. In the case of volcanic ash sand composed of coarse grains that do not have frost susceptibility, no frost heaving occurred and no ice lenses were observed. The gray levels of the frozen areas of the weathered volcanic ash and terrace deposits with frost susceptibility were found to decrease. This is thought to be because the precipitation of ice lenses in the soil pushed the soil particles apart and reduced their density relatively.

Keywords: Micro-focus X-ray CT scanner, Frost Heave, Ice lens, Observation, Density changes

1. INTRODUCTION

In recent years, industrial X-ray CT scanners, which have higher power than medical X-ray CT scanners and were developed for the purpose of detecting defects in industrial parts, have been widely used in universities and other research institutes. X-ray CT scanners are becoming more common in the research fields of geotechnical engineering. Some studies have attempted to elucidate the microstructure of soil [1,2] and to understand mechanical test results [3,4] by taking advantage of the X-ray CT scan's capabilities to observe the internal structure of materials nondestructively. For example, Higo et al. [3] successfully observed the strain localization behavior and the microstructural changes in partially saturated soil during the deformation process using microfocus X-ray CT scan. Watanabe et al. [4] measured the displacements in the soil under triaxial compression by tracking soil particles in the soil based on quantified X-ray CT data in three dimensions.

However, there are very few studies on X-ray CT scans of soil in a frozen state, compared to those of soil in an unfrozen state. For example, Fan et al. [5] investigated the impact of freeze-thaw on the macropore and fissure redistribution in clay by using X-ray CT scan. Wang et al. [6] reported a detailed study of structural change in clay due to freeze–thaw by using X-ray CT scan, and concluded that the technique can be an effective tool for examining detailed soil structural change.

The only previous study that used an X-ray CT scanner to observe the frost heaving process in soil is Torrance et al. [7]. This is because in order to perform an X-ray CT scan of soil during the frost heaving process, it is necessary to develop a compact experimental apparatus that can be set on the CT stage with accurate temperature control and moisture supply inside the X-ray CT scanner. Torrance et al. [7] developed an experimental apparatus that could freeze soil inside the X-ray CT scanner and observed its structural changes. However, they couldn't observe the ice lenses in detail owing to the somewhat large voxel size (43 μm) and low resolution.

This paper aims at developing a technique for observing the frost heaving process in soil nondestructively and microscopically using an industrial micro-focus X-ray CT scanner. For this purpose, a compact frost heaving apparatus that could freeze the soil in one dimension inside the X-ray CT scanner was developed. The X-ray CT scanner used for this study is equipped with a micro-focus X-ray generator and a high-sensitivity

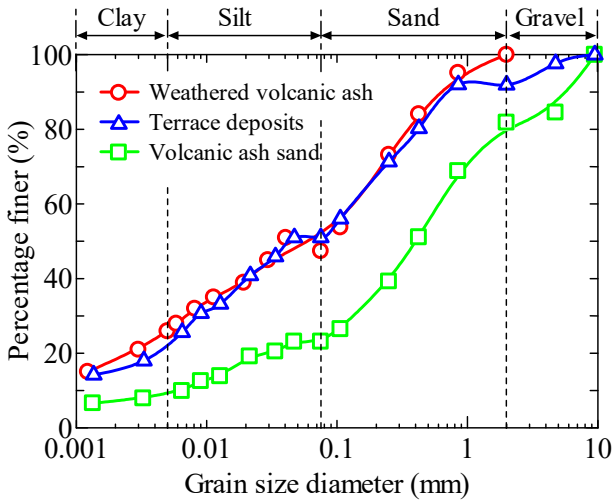

Fig.1 Grain size distributions

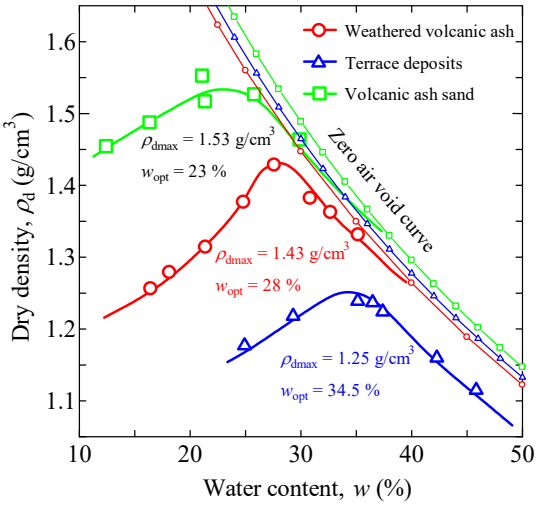

Fig.2 Compaction curves

Table 1 Physical properties of the soil samples

Soil sample	Grain size distribution (%)				Fine fraction content F_c (%)	Optimum water content w_{opt} (%)	Maximum dry density ρ_{dmax} (g/cm^3)	Soil particle density ρ_s (g/cm^3)
	Clay	Silt	Sand	Gravel				
Weathered volcanic ash	25	25	50	0	50	28.0	1.43	2.557
Terrace deposits	23	27	41	9	50	34.5	1.25	2.613
Volcanic ash sand	9	15	56	20	24	23.0	1.53	2.684

X-ray detector, which enables microscopic observation in frozen soil with a small voxel size (29 μm) and high resolution. This experimental method made it possible to observe the process of ice lens formation in the soil and the shape of the ice lens in detail. The X-ray CT scan images taken in this study are expected to help clarify the frost heaving mechanism of soil.

2. OUTLINE OF THE EXPERIMENT

2.1 Soil samples

In this study, three types of soil samples were used: weathered volcanic ash, terrace deposits, and volcanic ash sand.

Figure 1 shows the grain size distributions of soil samples obtained in accordance with the method stipulated by JIS A 1204. Weathered volcanic ash passed through a 2 mm sieve, and terrace deposits and volcanic ash sand passed through a 10 mm sieve were used for the experiments. In other words, the samples were conditioned so that the weathered volcanic ash contained no gravel and the terrace deposits and volcanic ash sand contained a small amount of gravel. However, the two types of samples, weathered volcanic ash and terrace deposits, have generally similar particle size distributions, especially for fine grains. On the other hand, volcanic ash sand has a different grain size distribution, with more coarse grains and fewer fine grains.

Figure 2 shows compaction curve of these samples obtained in accordance with the A-a method stipulated by JIS A 1210 (Compaction energy, E_c = 550 kJ/m^3 (Standard proctor)).

Table 1 shows the physical properties of the soil samples read from Fig. 1 and Fig. 2, plus the soil particle densities obtained in accordance with the method stipulated by JIS A 1202. Based on the coarse-grained and fine-grained contents and geological background, the soil samples are classified into two groups: volcanic ash sand and terrace deposits are classified as volcanic cohesive soil, and volcanic ash sand is classified as fine-grained gravelly sand.

2.2 Preparation of specimens

Table 2 Conditions for preparation of soil specimens

Soil sample	Water content w (%)	Wet density ρ_t (g/cm^3)	Dry density ρ_d (g/cm^3)	Void ratio e (%)	Degree of saturation S_r (%)
Weathered volcanic ash	28.0	1.74	1.36	0.88	81
Terrace deposits	34.5	1.60	1.19	1.20	75
Volcanic ash sand	23.0	1.80	1.45	0.85	73

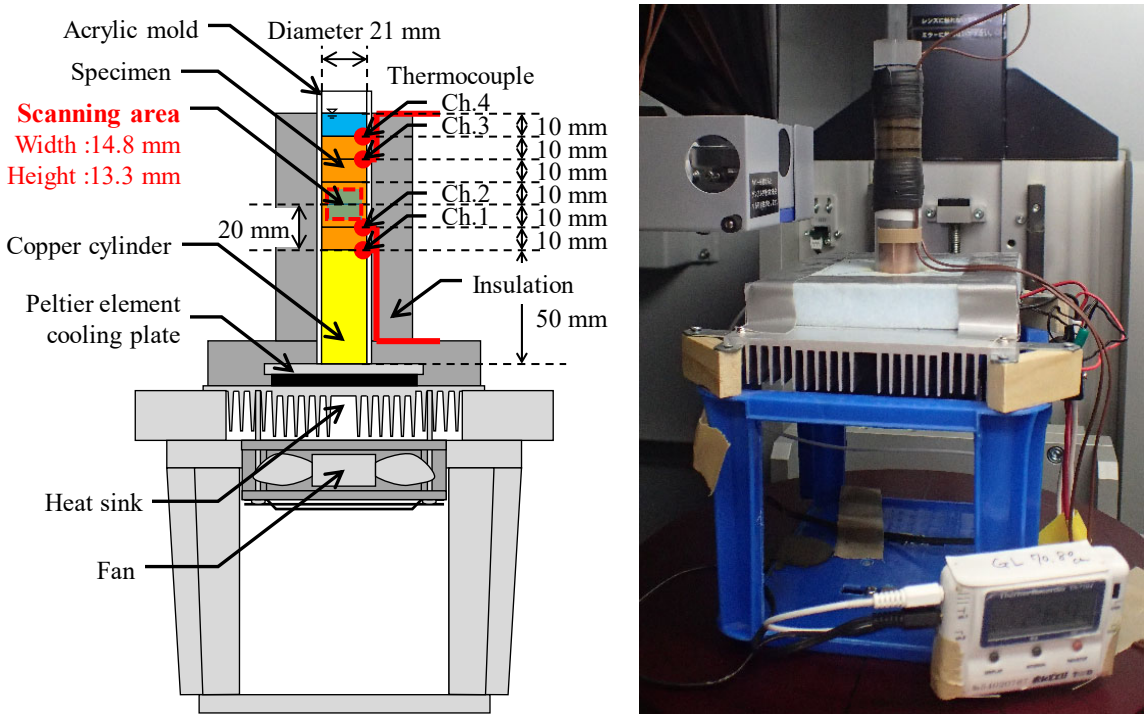

Fig.3 Compact frost heaving apparatus

Table 2 shows the conditions for preparation of soil specimens. In this study, compaction was performed using an acrylic mold and piston, and experiments were conducted on reconstituted specimens. The mold is cylindrical with an inner diameter of 21 mm. The diameter of specimen was made small to facilitate the penetration of X-rays. Water was added to naturally seasoned soil samples before thorough agitation. The soil sample necessary to obtain designated wet density for one layer was put into the mold, and a piston with almost the same cross section was inserted, and then hammered down the handle with a plastic hammer to make each layer the designated height of 10 mm. In each specimen, each compacted layer had a thickness of 10 mm, with five layers. Shapes of the specimens were columnar with a diameter of 21 mm and a height of 50 mm. And the degree of compaction is set to 95% for all types of soil samples.

2.3 Compact frost heaving apparatus

Figure 3 shows the compact frost heaving apparatus. Peltier cooling plate was used for freezing the specimens in this study. The Peltier cooling plate is connected to a temperature controller. This temperature controller can be connected to a 100 V AC socket and allows the temperature of the plate to be controlled between -10 and +70 °C. The specimens were cooled from the bottom in the same way as the Japanese Geotechnical Society standard [8]. The temperature of the cooling plate during freezing was controlled at -10 °C to prevent the specimen from becoming supercooled. The temperature of the top surface of the specimen is not controlled. The water required for frost heaving is supplied from the top of the specimen. The temperature of the water is the same as room temperature, +25 °C. The side of the specimen is insulated to avoid the influence of room temperature.

During the experiment, the temperatures at the bottom and top of the specimen and the internal temperatures of the specimen are measured by four thermocouples (Ch.1, Ch.2, Ch.3, and Ch.4) installed as shown in Fig. 3. The measured temperature data are recorded every minute by a data logger installed outside the X-ray CT scanner.

The X-ray CT scan images were taken at 20 mm from the bottom of the specimen, with a width of 14.8 mm and a height of 13.3 mm. The imaging was carried out in half-scan mode (stage rotated 180 °) owing to the wiring of the power cable.

2.4 X-ray CT scan

2.4.1 Principle of the X-ray CT scan

In this section, the basic principles of X-ray CT scanning are described in detail. First, an X-ray tube emits a beam of X-rays, which is scanned in several directions over a selected surface, while a detector receives and measures the amount of X-rays transmitted. This value is then converted into a digital signal by an analogue-to-digital converter and transferred to a computer for storage and calculation. At this point, the X-ray attenuation values for each unit volume of the plane are obtained. The attenuation values are then converted into an X-ray CT scan image by computer back-projection reconstruction via a digital-to-analogue converter. Finally, the X-ray CT scan image is shown on the display.

2.4.2 CT value

This chapter describes in detail the CT values widely used for the interpretation of X-ray CT scans, with reference to Higo et al. [3]. In this study, the CT value is expressed as the luminance value (gray level) of the X-ray CT scan image. Lighter colors in the X-ray CT scan image indicate areas where the attenuation coefficient of the object is large, while darker colors indicate areas where the attenuation coefficient is small. In other words, the X-ray CT scan image can be thought of as a two-dimensional distribution of the X-ray attenuation coefficient of a certain scanning plane of the object.

The attenuation coefficient of the X-rays to be taken is defined by the following equation (Higo et al. [3]):

$$\mu = \mu_m \rho \tag{1}$$

where μ is the attenuation coefficient of the X-ray to be scanned, μ_m is the mass attenuation coefficient specific to the material, and ρ is the density of the material. This indicates that for the same material, the higher the density, the higher the X-ray attenuation rate. Therefore, the X-ray CT scan image can be considered as a density distribution map, and the changes in density of a material during an experiment can be quantitatively expressed as changes in CT value.

2.4.3 Overview of the X-ray CT scanner used in this study

Figure 4 shows the structure of the X-ray CT scanner. The X-ray CT scanner used in this study is the Shimadzu inspeXio SMX-225CT. The system is equipped with a micro-focus X-ray generator, an image intensifier and a high-precision stage.

Table 3 shows the main specifications of this system.

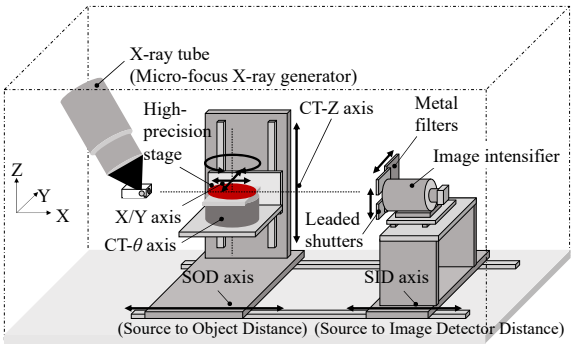

Fig.4 Structure of the X-ray CT scanner

Table 3 Main specifications of X-ray CT scanner used in this study

Maximum tube voltage (kV)	225
Maximum tube current (μA)	1000
Rated power (W)	135
Image resolution (μm)	4
Maximum sample size (mm)	ϕ300×h300
Maximum sample weight (kg)	9
Visual field of detector (inch)	9 / 7.5 / 6 / 4.5
Pixel size	1024×1024

2.4.4 Installation of the frost heaving apparatus inside the X-ray CT scanner and the conditions for the X-ray CT scan

Figure 5 shows the X-ray CT scanner and the frost heaving apparatus installed inside the system. The frost heaving apparatus was fixed on the CT stage as shown in the figure, and the X-ray CT scan images were taken while the soil was frozen.

Table 4 summarizes the X-ray CT scan conditions for this study. The X-ray CT scans were performed at a tube voltage of 160 kV, a tube current of 40 μA and a voxel size of 29 μm.

2.4.5 Overview of the Analysis software used in this study

In this study, ExFact VR 2.0 (Nihon Visual Science, Inc.), a three-dimensional analysis software, was used to observe the frost heaving

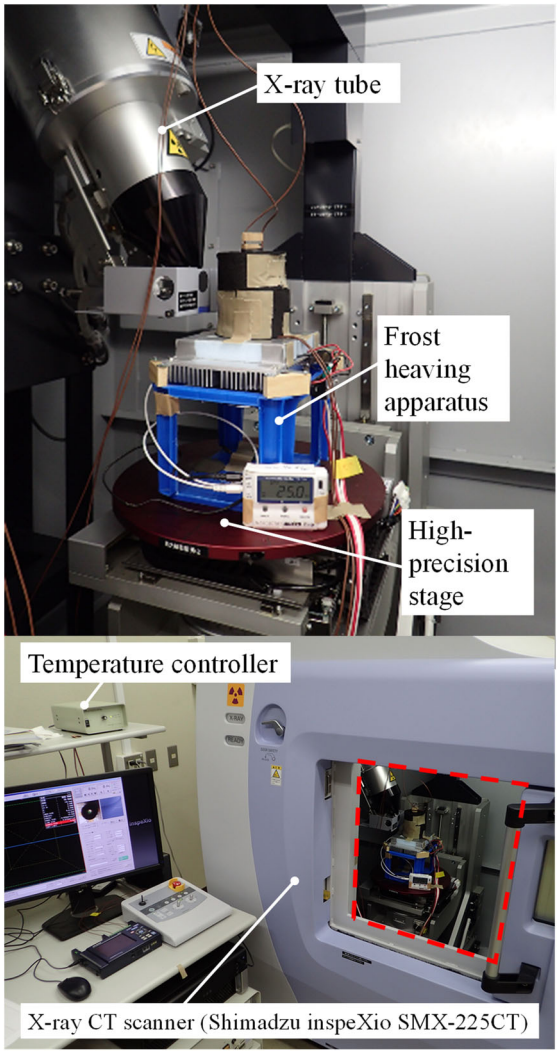

Fig.5 X-ray CT scanner and the frost heaving apparatus installed inside the system.

process in soil. This analysis software allows the visualization of tomographic images obtained from X-ray CT scans in two or three dimensions by means of volume rendering.

An X-ray CT scan outputs a series of tomographic images as digital data. The CT data is an array of solutions obtained by collecting the signals of the electromagnetic waves detected through transmission/attenuation/scattering on a rotating sample and then mathematically reconstructing them. This analysis software considers the array as pixels, associates luminance information, sets the contrast for easy viewing, and displays it as an image.

3. RESULTS AND DISCUSSIONS

3.1 Changes in frost heave amounts, water absorptions and temperatures with time

Table 4 X-ray CT scan conditions for this study

Tube voltage (kV)	160
Tube current (μA)	40
Voxel size (μm)	29
Pixel size	512×512
Number of views	3600
Number of averages	10

Figure 6 shows the changes in frost heave amounts, water absorptions and temperatures of the specimens with time for the three types of soil samples. It can be seen that the temperature changes (and temperature gradient) during freezing are generally similar in all experiments. Specifically, the internal temperatures of the specimens can be found to be +13 °C, +10 °C, -4 °C, and -10 °C, in order from top to bottom. The measurements of the soil temperatures show that when the temperature changes are in equilibrium, the position of the X-ray CT scan imaging (see Fig. 3) is located in the region containing 0°C between the thermocouples of Ch.2 and Ch.3.

As mentioned above, despite similar temperature gradients during freezing, significant differences were observed in the frost heave amounts. The frost heave amounts are measured by reading the positions of the top surface of the specimens from the X-ray scan images. Comparing the frost heave amounts for each soil sample, it could be confirmed that weathered volcanic ash reached 6.2 mm after 24 h, terrace deposits reached 5.5 mm after 48 h, and volcanic ash sand reached just 2 mm after 26 h from the start of freezing. These results were related to the fine fraction contents shown in Table 1. Both weathered volcanic ash and terrace deposits have fine fraction contents of about 50 %, which are much higher than that of volcanic ash sand (fine fraction content of 24 %). In other words, it was confirmed that the frost heave amount tended to increase with the increase of fine fraction content. These results are consistent with the results of Konrad [9], which reported the segregation potential, hence frost susceptibility, of soils was related to the average size of the fines fraction.

Furthermore, it can be seen that the amount of frost heave does not change at around 5 mm for both weathered volcanic ash and terrace deposits. Since the bottom of the specimen was cooled at a constant temperature, it was considered that the cooling of the apparatus and the latent heat in the specimen reached thermal equilibrium when the frost heave amount reached about 5 mm. If the bottom of the specimen can be cooled at a constant rate, the frost heave phenomenon is expected to still continue.

The frost heave rates are the time variation of the frost heave amounts and are calculated by the

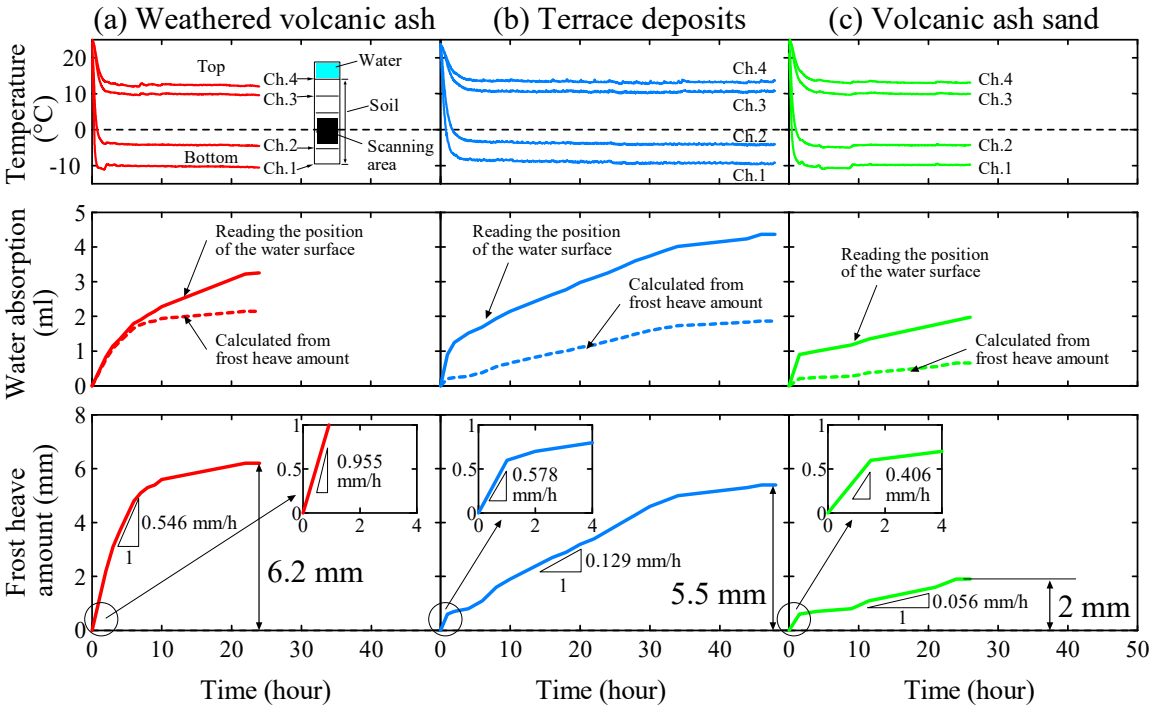

Fig.6 Changes in frost heave amounts, water absorptions and temperatures of the specimens with time for the three types of soil samples

slope of the line in Fig. 6. It can be seen that the frost heave rate increases rapidly after the freezing starts (within one hour) for all soil samples. The specific frost heave rates were 0.955 mm/h for weathered volcanic ash, 0.578 mm/h for terrace deposits, and 0.406 mm/h for volcanic ash sand. At this time, the internal temperature of the specimen is rapidly dropping from room temperature, and the freezing front (0 °C) is moving upward at a high speed. Since there is no heat balance inside the specimen, thick ice lenses are not formed, but thin ice lenses are formed continuously as the freezing front moves.

On the other hand, it can be seen that the frost heave rates of each specimen changed significantly after one hour of the experiment. The specific frost heave rates were 0.546 mm/h for weathered volcanic ash, 0.129 mm/h for terrace deposits, and 0.056 mm/h for volcanic ash sand. In weathered volcanic ash and terrace deposits, the soil begins to absorb water from the outside due to the occurrence of ice lenses, and this process is thought to determine the total frost heave amount. It can also be confirmed that the frost heave rate is in good agreement with the fine fraction content shown in Table 1. The frost heave rate of the weathered volcanic ash was somewhat higher than that of the terrace deposits, which may be attributed to the 9 % gravel content of the terrace deposits. These results are consistent with the results of Casagrande [10] and Kapler [11], which clarified the relationship between frost susceptibility and grain size distribution.

It can be seen that the changes in water absorption during the experiments are in good agreement with the changes in frost heave amounts. As in the case of frost heave amounts, the water absorption was also measured by reading the position of the water surface on the specimen using X-ray CT scan images. However, for all soil samples, the water absorptions from readings were higher than the water absorption calculated from the frost heave amounts. In this experiment, the specimens were frozen from an unsaturated state, and most of the water absorption was considered to have been absorbed into the pores in the soil on the unfrozen side.

3.2 Observation of the frost heaving process in soil

Figure 7 summarizes the 3D reconstructed images of each specimen during the frost-heaving process obtained by the X-ray CT scans. As mentioned above, in the X-ray CT scan image, luminance is represented by shading, with low-density areas shown in black and high-density areas shown in white. Therefore, low-density materials such as ice and water are represented in black, and high-density materials such as soil particles are represented in white. As shown in Fig. 7, we succeeded in observing the process of ice-lens formation in the soil and the shape of the ice lens in detail by using this experimental method.

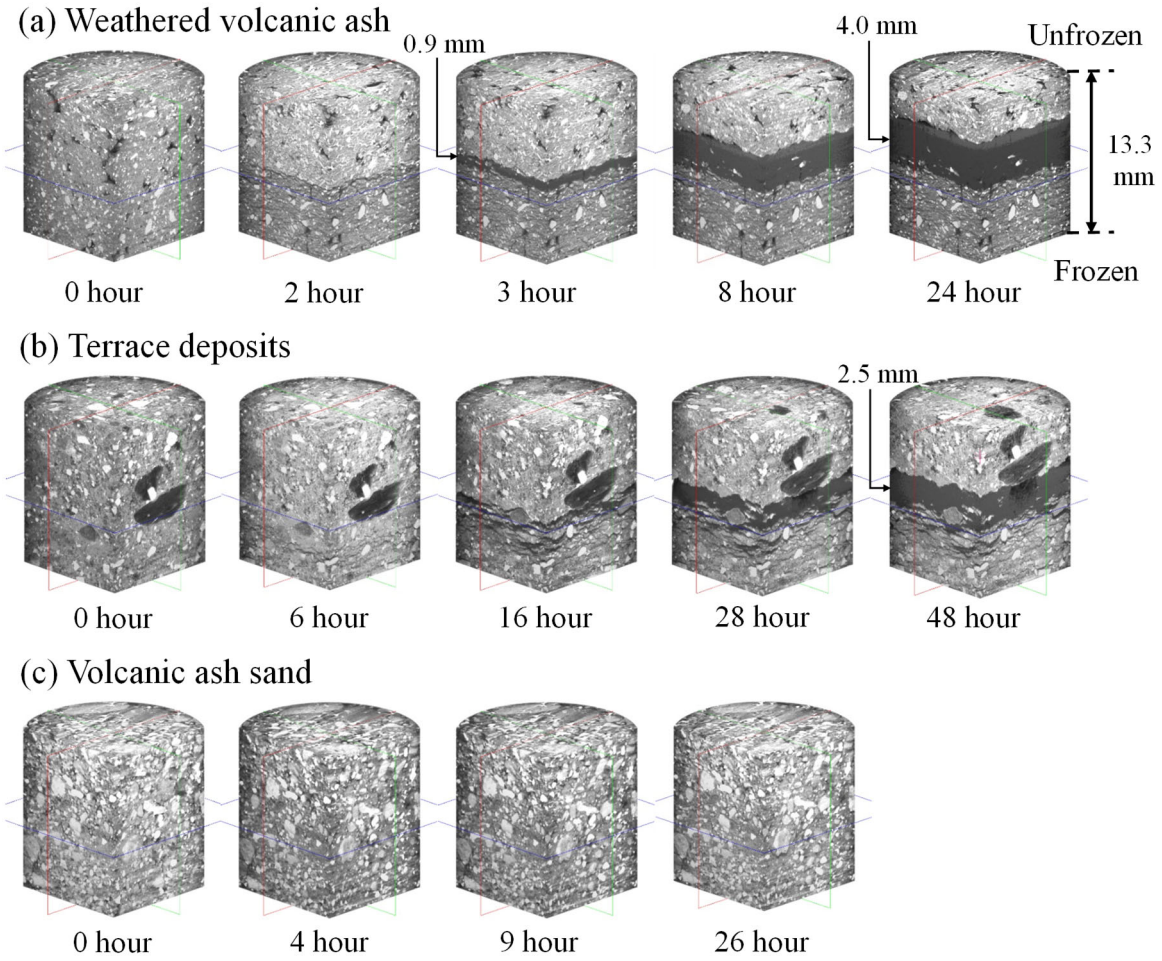

Fig.7 3D reconstructed images of each specimen during the frost heaving process obtained by the X-ray CT scans

Figure 7 (a) shows that the freezing front is still moving in the weathered volcanic ash until two hours after the start of the experiment, and multiple ice lenses like cracks are generated. After three hours, the freezing front began to stagnate, and it was confirmed that a thick ice lens gradually began to grow, and after 24 hours, it was observed that the ice lens had grown to about 4 mm thick. It was also observed that the weathered volcanic ash without gravel content formed relatively flat shaped ice lenses.

Figure 7 (b) shows that one distinct ice lens occurs in the terrace deposits after 16 hours of the experiment. Although the ice lens grew over time, the growth rate was slow. Even after 48 hours of experimentation, its thickness had reached only about 2.5 mm. However, the growth of ice lenses like cracks can be observed in the frozen region below the thick ice lens in the terrace deposits. In the terrace deposits containing gravel, ice lenses were observed to form from around larger particles, and the ice lenses were more uneven in shape than weathered volcanic ash.

Figure 7 (c) shows that no ice lenses were formed in the volcanic ash sand, and only thin cracks were observed after 26 hours of the experiment. This is probably the reason that the volcanic ash sand is composed of coarse grains that are non-frost susceptible.

Furthermore, the 3D reconstructed image in Fig. 7 was sliced in a cylindrical shape with a thickness of 0.317 mm (11 voxels), and the average of the luminance value (gray level) of each slice was calculated to determine the change in the height direction of the specimen. As mentioned earlier, the luminance value, which is the output value in an X-ray scan, is correlated with the amount of X-ray attenuation, so the luminance value and the increase or decrease in density can be considered to correspond.

Figure 8 shows the changes in gray level in the height direction for each specimen. The maximum and minimum grey levels are determined by the densities of the materials contained in the X-ray CT scan images and therefore differ for each soil sample. From the changes in gray level, it can be

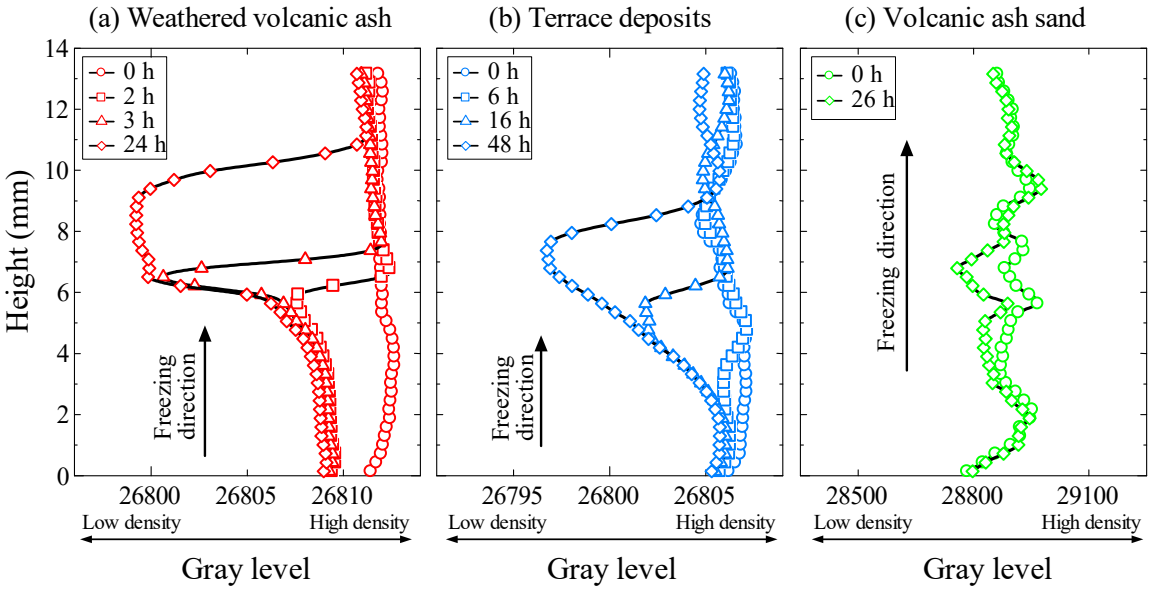

Fig.8 Changes of gray Level in the height direction for each specimen

seen that the freezing front moves to a position with a height of 6 mm in the weathered volcanic ash two hours after the start of the experiment, and the density of the frozen area decreases (Fig. 8 (a)). This is thought to be because the precipitation of ice lenses in the soil pushed the soil particles apart and reduced their density relatively. Three hours after the start of the experiment, it can be seen that ice lenses have begun to form owing to the moisture that has absorbed on the freezing front. After 24 hours, the ice lens gradually grew into a thick ice lens of about 4 mm. Similar to the weathered volcanic ash, the freezing front of the terrace deposits moved to the position of 4 mm in height after six hours of the experiment, and the density of the frozen area decreased (Fig. 8 (b)). On the other hand, the gray level of volcanic ash sand did not change because the soil was coarse-grained and did not have frost susceptibility (Fig. 8 (c)).

4. CONCLUSIONS

In this paper, a compact frost heaving apparatus that could freeze the soil in one dimension was developed to observe the frost heaving process in soil nondestructively and microscopically using industrial micro-focus X-ray CT scanner. This experimental method made it possible to observe the process of ice lens formation in the soil and the shape of the ice lens in detail. And it was also able to understand that the changes in soil densities associated with the formation of ice lenses by observing the changes in gray level obtained from X-ray CT scan images. The main results are as follows:

1) In highly frost susceptible weathered volcanic ash, ice lenses like multiple cracks were observed to develop in the early stages of the experiment. When the freezing front was stagnant and the heat was balanced, thick and well-developed ice lenses could be observed. The shape of the ice lens observed in the weathered volcanic ash without gravel was relatively flat.
2) In the terrace deposits containing gravel, ice lenses were observed to be formed from around the larger particles. Furthermore, the formed ice lenses were more uneven in shape than weathered volcanic ash.
3) In the case of volcanic ash sand composed of coarse grains that do not have frost susceptibility, no frost heaving occurred and no ice lenses were observed.
4) The gray levels of the frozen areas of the weathered volcanic ash and terrace deposits with frost susceptibility were found to decrease. This is thought to be because the precipitation of ice lenses in the soil pushed the soil particles apart and reduced their density relatively.

From these results, it is clear that the X-ray CT scan is an effective means of understanding the effects of frost heaving on soil.

5. REFERENCES

[1] Hamamoto S., Moldrup P., Kawamoto K., Sakaki T., Nishimura T. and Komatsu T., Pore Network Structure Linked by X-ray CT to Particle Characteristics and Transport Parameters, Soils and Foundations, Vol. 56, Issue 4, 2016, pp. 676-690.

[2] Minabe Y., Kawajiri S., Kawaguchi T., Nakamura D. and Yamashita S., Correlation between Mechanical Properties and Suction

Calculated by X-ray CT of Unsaturated Sandy Soil, Procedia Engineering, Vol. 143, 2016, pp. 292-299.

[3] Higo Y., Oka F., Kimoto S., Sanagawa T. and Matsushima Y., Study of Strain Localization and Microstructural Changes in Partially Saturated Sand during Triaxial Tests Using Microfocus X-ray CT, Soils and Foundations, Vol. 51, Issue 1, 2011, pp. 95-111.

[4] Watanabe Y., Lenoir N., Otani J. and Nakai T., Displacement in Sand Under Triaxial Compression by Tracking Soil Particles on X-ray CT Data, Soils and Foundations, Vol. 52, Issue 2, 2012, pp. 313-320.

[5] Fan W., Yang P. and Yang J.Z., Freeze-Thaw Impact on Macropore Structure of Clay by 3D X-ray Computed Tomography, Engineering Geology, Vol. 280, 2021, Article 105921.

[6] Wang S., Yang J.Z. and Yang P., Structural change and volumetric shrinkage of clay due to freeze-thaw by 3D X-ray computed tomography, Cold Regions Science and Technology, Vol. 138, 2017, pp. 108-116.

[7] Torrance J.K., Elliot T., Martin R., Heck R. J., X-ray Computed Tomography of Frozen Soil, Cold Regions Science and Technology, Vol. 53, 2008, pp. 75-82.

[8] Japanese Geotechnical Society, JGS 0172-2009, Test Method for Frost Susceptibility of Soils, 2011.

[9] Konrad J.M., Frost Susceptibility Related to Soil Index Properties, Canadian Geotechnical Journal, Vol. 36, No. 3, 1999, pp. 403-417.

[10] Casagrande A., Discussion on a New Theory of Frost Heaving by Benkelman and Olmstead, Highway Research Board Proceedings, Vol. II, pt. 1, 1932, pp. 168-172.

[11] Kaplar C. W., A Laboratory Freezing Test to Determine the Frost Susceptibility of Soils, CRREL Technical Report, No. 250, 1974, pp. 1-36.